
Gaussian Process Bandit Optimization of the Thermodynamic Variational Objective

Vu Nguyen

University of Oxford
vu@robots.ox.ac.uk

Vaden Masrani

University of British Columbia
vadmas@cs.ubc.ca

Rob Brekelmans

USC Information Sciences Institute
brekelma@usc.edu

Michael A. Osborne

University of Oxford
mosb@robots.ox.ac.uk

Frank Wood

University of British Columbia
fwood@cs.ubc.ca

Abstract

Achieving the full promise of the Thermodynamic Variational Objective (TVO), a recently proposed variational lower bound on the log evidence involving a one-dimensional Riemann integral approximation, requires choosing a “schedule” of sorted discretization points. This paper introduces a bespoke Gaussian process bandit optimization method for automatically choosing these points. Our approach not only automates their one-time selection, but also dynamically adapts their positions over the course of optimization, leading to improved model learning and inference. We provide theoretical guarantees that our bandit optimization converges to the regret-minimizing choice of integration points. Empirical validation of our algorithm is provided in terms of improved learning and inference in Variational Autoencoders and Sigmoid Belief Networks.

1 Introduction

The Variational Autoencoder (VAE) framework has formed the basis for a number of recent advances in unsupervised representation learning [18, 36, 42]. Assuming a generative model involving latent variables, VAEs perform maximum likelihood parameter estimation by optimizing the tractable Evidence Lower Bound (ELBO) on the logarithm of the model evidence. In doing so, the VAE framework introduces an inference network, which seeks to approximate the true posterior over latent variables. While the ELBO is a common choice of variational inference objective, recent work has sought to improve the model learning [7, 39, 31, 26] or inference aspects [35, 19, 8, 13] of this task.

In this work, we build upon the recent Thermodynamic Variational Objective (TVO), which frames log-likelihood estimation as a one-dimensional integral over the unit interval [27]. The integral is estimated using a Riemann sum approximation, as visualized in Figure 1, yielding a natural family of variational inference objectives which generalize and tighten the ELBO.

The choice of a d -dimensional vector of points $\beta = [\beta_0, \beta_1, \dots, \beta_{d-1}]^T$ at which to construct this numerical approximation is an important hyperparameter for the TVO, which we refer to as an “integration schedule” throughout this work. Previous work [27] uses a static integration schedule, and requires grid search over the choice of initial β_1 . However, since the shape of the integrand reflects the quality of the inference network (§2), recent work [6] suggests that this scheduling procedure may be improved by dynamically choosing β over the course of training. Our proposed approach also allows the TVO to be adapted to different model architectures and schedule dimensionality without the need for grid search.

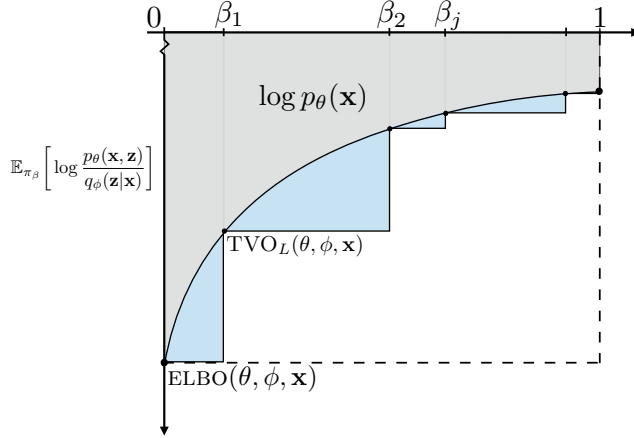


Figure 1: The TVO objective frames log likelihood estimation as a Riemann sum approximation to a 1-d integral, with the ELBO as a special case for a single $\beta_0 = 0$. The TVO (area in blue) bounds the integral more tightly than the ELBO (area within dotted lines).

Our primary contribution is to automate the choice of integration schedules using a Gaussian process bandit optimization. We first demonstrate that maximizing the TVO objective as a function of β is equivalent to a regret-minimization problem, where the black-box reward function reflects improvement in the objective for a given choice of schedule. We model this reward function over the course of training epochs using a time-varying Gaussian process (GP). Our entire procedure amounts to 1) choosing β to maximize an acquisition function in our surrogate GP model, 2) observing the reward function as the improvement in the TVO objective over one or more epochs of training with the chosen schedule, and 3) using these observations to update the GP model and select a new β . Our bandit algorithm is optimal in the sense of converging to a global regret-minimizing solution, as in the time-varying GP bandit optimization approach [5]. By choosing β to maximize an acquisition function that balances exploration and performance, our algorithm achieves global guarantees despite the non-convexity of the reward function. Further, our approach is directly aligned with the goal of improved model learning and inference, as the bandit reward function tracks the variational objective over the course of training.

We review the TVO framework in §2, before presenting our bandit optimization approach in §3. We provide details of our time-varying Gaussian process model and discuss its convergence properties in §4. Finally, we demonstrate that our method can improve both model learning and inference in Variational Autoencoders and Sigmoid Belief Networks, in §5.

2 The Thermodynamic Variational Objective (TVO)

Assuming a generative model $p_\theta(\mathbf{x}, \mathbf{z})$, we are interested in maximizing the log-likelihood $\log p_\theta(\mathbf{x}) = \log \int p_\theta(\mathbf{x}, \mathbf{z}) d\mathbf{z}$ over parameters θ , given the empirical data \mathbf{x} . However, this is intractable due to the integral over the latent variables \mathbf{z} . Variational inference methods [4] often seek to maximize the tractable ELBO instead, obtained by introducing an approximate posterior $q_\phi(\mathbf{z} | \mathbf{x})$ and optimizing the objective

$$\text{ELBO}(\theta, \phi, \mathbf{x}) = \log p_\theta(\mathbf{x}) - D_{\text{KL}}[q_\phi(\mathbf{z} | \mathbf{x}) || p_\theta(\mathbf{z} | \mathbf{x})] = \mathbb{E}_{q_\phi(\mathbf{z} | \mathbf{x})} \left[\log \frac{p_\theta(\mathbf{x}, \mathbf{z})}{q_\phi(\mathbf{z} | \mathbf{x})} \right]. \quad (1)$$

Thermodynamic Integration (TI) [33, 10, 11] is a common technique for estimating (ratios of) partition functions in statistical physics, which instead frames estimating $\log p_\theta(\mathbf{x})$ as a one-dimensional integral over a geometric mixture curve parameterized by β .¹ In particular, for the TVO, this curve interpolates between the approximate posterior $q_\phi(\mathbf{z} | \mathbf{x})$ and true posterior $p_\theta(\mathbf{z} | \mathbf{x})$. Following [6]

¹Here β is a scalar to be consistent with notation in [27]. In the remainder of the paper, we let β hold the sorted vector of discretization points $\beta = [\beta_0, \beta_1, \dots, \beta_{d-1}]^T$, so that each β_j specifies a $\pi_{\beta_j}(\mathbf{z} | \mathbf{x})$ in (2).

this mixture curve can be interpreted as an exponential family of distributions over \mathbf{z} given \mathbf{x}

$$\pi_\beta(\mathbf{z} | \mathbf{x}) = q_\phi(\mathbf{z} | \mathbf{x}) \exp\{\beta \cdot \log \frac{p_\theta(\mathbf{x}, \mathbf{z})}{q_\phi(\mathbf{z} | \mathbf{x})} - \log Z_\beta(\mathbf{x})\} \quad (2)$$

$$\text{where } Z_\beta(\mathbf{x}) = \int q_\phi(\mathbf{z} | \mathbf{x})^{1-\beta} p_\theta(\mathbf{x}, \mathbf{z})^\beta d\mathbf{z} .$$

Noting that $\log Z_0(\mathbf{x}) = 0$ and $\log Z_1(\mathbf{x}) = \log p_\theta(\mathbf{x})$, TI now applies the fundamental theorem of calculus to write the model evidence as an integral

$$\log p_\theta(\mathbf{x}) - 0 = \int_0^1 \frac{\partial}{\partial \beta} \log Z_\beta(\mathbf{x}) d\beta = \int_0^1 \mathbb{E}_{\pi_\beta} \left[\log \frac{p_\theta(\mathbf{x}, \mathbf{z})}{q_\phi(\mathbf{z} | \mathbf{x})} \right] d\beta, \quad (3)$$

where we have used the known property of exponential families [44] that the derivative of $\log Z_\beta(\mathbf{x})$ with respect to β matches the expected sufficient statistics [27, 6]. Masrani et al. [27] use self-normalized importance sampling (SNIS) to estimate each term in the integrand, with S importance samples and $q_\phi(\mathbf{z} | \mathbf{x})$ as the proposal for each β

$$\mathbb{E}_{\pi_\beta}[\cdot] \approx \frac{\sum_{\ell=1}^S w_\ell^\beta}{\sum_{\ell=1}^S w_\ell^\beta} [\cdot], \quad w_\ell = \frac{p_\theta(\mathbf{x}, \mathbf{z}_\ell)}{q_\phi(\mathbf{z}_\ell | \mathbf{x})}, \quad \mathbf{z}_\ell \sim q_\phi(\mathbf{z} | \mathbf{x}). \quad (4)$$

Since $\log Z_\beta(\mathbf{x})$ is convex [44], we know that the integrand in (3) is an increasing function of β . Thus, we can obtain lower and upper bounds using left- and right-Riemann sums, respectively, over a discrete partition β of the unit interval. The left-Riemann sum then defines the TVO lower bound

$$\text{TVO}(\theta, \phi, \beta, \mathbf{x}) := \sum_{j=0}^{d-1} (\beta_{j+1} - \beta_j) \mathbb{E}_{\pi_{\beta_j}} \left[\log \frac{p_\theta(\mathbf{x}, \mathbf{z})}{q_\phi(\mathbf{z} | \mathbf{x})} \right], \quad (5)$$

where $\beta = [\beta_j]_{j=0}^{d-1}$ with $\beta_0 = 0$ and $\beta_j < \beta_{j+1}$. Note that the single-term left-Riemann sum with $\beta = \beta_0 = 0$ matches the ELBO in (1), since $\pi_0(\mathbf{z} | \mathbf{x}) = q_\phi(\mathbf{z} | \mathbf{x})$. However, how to choose intermediate β_j for $d > 1$ remains an interesting question, which we proceed to frame as a bandit problem.

3 From Evidence Maximization to Regret Minimization

We view the vector $\beta \in [0, 1]^d$ as an arm [1] to be pulled in a continuous space, given a fixed resource of T training epochs. After each round, we receive an estimate of the log evidence \mathcal{L} , from which we will construct a reward function. An important feature of our problem is that the integrand in Figure 1 changes between rounds as training progresses. Thus, our multi-armed bandit problem is said to be *time-varying*, in that the optimal arm and reward function depend on round t .

More formally, we define the time-varying reward function $f_t : [0, 1]^d \rightarrow \mathbb{R}$ which takes an input β_t and produces reward $f_t(\beta_t)$. At each round we get access to a noisy reward $y_t = f_t(\beta_t) + \epsilon_t$ where we assume Gaussian noise $\epsilon_t \sim \mathcal{N}(0, \sigma_f^2)$. We aim to maximize the cumulative reward $\sum_{t=1}^{T/w} f_t(\beta_t)$ across T/w rounds, where w is a divisor of T and will later control the ratio of bandit rounds t to training epochs i .

Maximizing the cumulative reward is equivalent to minimizing the *cumulative regret*

$$R_{T/w} := \sum_{t=1}^{T/w} f_t(\beta_t^*) - f_t(\beta_t), \quad (6)$$

where $r_t := f_t(\beta_t^*) - f_t(\beta_t)$ is the *instantaneous regret* defined by the difference between the received reward $f_t(\beta_t)$ and maximum reward attainable $f_t(\beta_t^*)$ at round t . The regret, which is non-negative and monotonic, is more convenient to work with than the cumulative reward and will allow us to derive upper bounds in §4.3.

In order to translate the problem of maximizing the log evidence as a function of β into the bandits framework, we define a time-varying reward function $f_t(\beta_t)$. We construct this reward in such a way

Algorithm 1 GP-bandit for TVO (high level)

Input: schedule dimension d , reward function $f_t(\beta_t)$ where $\beta_t \in [0, 1]^d$, update frequency w

- 1: **for** $t = 1 \dots T$ **do**
- 2: Train the TVO and get \mathcal{L}_t from Eq. (5) given previously obtained β_{t-1}
- 3: **if** $\text{mod}(t, w) = 0$: time to update β_t **then**
- 4: Estimate the utility $y_t = \mathcal{L}_t - \mathcal{L}_{t-w}$ and augment $D_t = D_{t-1} \cup (\beta_{t-1}, t, y_t)$
- 5: Fit a time-varying, permutation invariant GP to D_t
- 6: Estimate $\mu_t(\beta), \sigma_t(\beta)$ from Eqs. (15,16)
- 7: Select $\beta_t = \arg \max \mu_t(\beta) + \sqrt{\kappa_t} \sigma_t(\beta)$ where κ_t is from Theorem 1
- 8: **end if**
- 9: **end for**

that minimizing the cumulative regret is equivalent to maximizing the final log evidence estimate $\mathcal{L}_T := \log p_{\theta_T}(\mathbf{x})$, i.e., such that $\min R_{T/w} = \max \mathcal{L}_T$.

Such a reward function can be defined by partitioning the T training epochs into windows of equal length w , and defining the reward for each window $t \in \{0, 1, \dots, T/w - 1\}$

$$f_t(\beta_t) := \mathcal{L}_{w(t+1)} - \mathcal{L}_{wt} \quad (7)$$

as the difference between the TVO log evidence estimate one window-length in the future $\mathcal{L}_{w(t+1)}$ and the present estimate \mathcal{L}_{wt} . Then, the cumulative reward is given by a telescoping sum over windows

$$\sum_{t=0}^{T/w-1} f_t(\beta_t) = (\mathcal{L}_w - \mathcal{L}_0) + (\mathcal{L}_{2w} - \mathcal{L}_w) + \dots + (\mathcal{L}_{(T/w)w} - \mathcal{L}_{(T/w-1)w}) \quad (8)$$

$$= \mathcal{L}_T - \mathcal{L}_0, \quad (9)$$

where \mathcal{L}_0 is the initial (i.e. untrained) loss. Recalling the definition of cumulative regret in Eq. (6),

$$\min R_{T/w} = \min \left(\sum_{t=0}^{T/w-1} f_t(\beta_t^*) \right) - \left(\sum_{t=0}^{T/w-1} f_t(\beta_t) \right) \quad (10)$$

$$= \min \left((\mathcal{L}_T^* - \mathcal{L}_0) - (\mathcal{L}_T - \mathcal{L}_0) \right) \quad (11)$$

$$= \min (\text{const} - \mathcal{L}_T) \quad (12)$$

$$= \max \mathcal{L}_T. \quad (13)$$

Therefore minimizing the cumulative regret for the reward function defined by Eq. (7) is equivalent to maximizing the log evidence on the final epoch. Next, we describe how to design an optimal decision mechanism to minimize the cumulative regret $R_{T/w}$ using Gaussian processes.

4 Minimizing Regret with Gaussian Processes

There are two unresolved problems with the reward function defined in Eq. (7) which still must be addressed. The first is that it is not in fact computable, due to its use of future observations. The second is that it ignores the ordering constraint required for β to be a valid Riemann partition.

We can handle both by problems by using a permutation-invariant Gaussian process to form a surrogate for the reward function $f_t(\beta_t)$. The surrogate model will be updated by past rewards, and used in place of $f_t(\beta_t)$ to select the next schedule at the current round, as described in Algorithm 1.

In §4.1 we formally define how to use (time-varying) Gaussian processes in bandit optimization, before describing how our permutation-invariant kernel can be used to solve the problem of ordering constraints on β in §4.2. Finally in §4.3 we provide a theoretical guarantee that our bandit optimization will converge to the regret-minimizing choice of β .

4.1 Time-varying Gaussian processes for Bandit Optimization

A popular design in handling time-varying functions [21, 41, 20, 32] such as $f_t(\boldsymbol{\beta}_t)$ is to jointly model the spatial and temporal dimensions using a product of covariance functions $k = k_\beta \otimes k_T$, where $k_\beta : [0, 1]^d \times [0, 1]^d \rightarrow \mathbb{R}$ is a spatial covariance function over actions, $k_T : \mathbb{N} \times \mathbb{N} \rightarrow \mathbb{R}$ is a temporal covariance function, and $k : \mathbb{R}_+^{d+1} \times \mathbb{R}_+^{d+1} \rightarrow \mathbb{R}$.

Under this joint modeling framework, the GP is defined as follows. At round t we have the history of rewards $\mathbf{y}_t = [y_0, \dots, y_t]^T$ and sample points $\mathbf{X}_t = \{\mathbf{x}_0, \dots, \mathbf{x}_t\}$, where we define $\mathbf{x}_t \in \mathbb{R}^{d+1}$ to be the concatenation of $\boldsymbol{\beta}_t$ and timestep t , i.e. $\mathbf{x}_t := [\boldsymbol{\beta}_t, t]^T$. Then the time-varying reward function is GP-distributed according to

$$f_t \sim GP(0, k(\mathbf{x}, \mathbf{x}')) \quad \text{where } k(\mathbf{x}, \mathbf{x}') := k_\beta(\boldsymbol{\beta}, \boldsymbol{\beta}') \times k_T(t, t'), \quad (14)$$

where we have assumed zero prior mean for simplicity. For theoretical convenience we follow [5] and choose $k_T(t, t') = (1 - \omega)^{\frac{|t-t'|}{2}}$, where ω is a ‘‘forgetting-remembering’’ trade-off parameter learned from data. We describe $k_\beta(\boldsymbol{\beta}, \boldsymbol{\beta}')$ in §4.2.

Using standard Gaussian identities [3, 34], the posterior predictive is also GP distributed, with mean and variance given by

$$\boldsymbol{\mu}_t(\boldsymbol{\beta}_*) = \mathbf{k}_t(\boldsymbol{\beta}_*)^T (\mathbf{K}_t + \sigma_f^2 \mathbf{I})^{-1} \mathbf{y}_t \quad (15)$$

$$\sigma_t^2(\boldsymbol{\beta}_*) = \mathbf{k}_t(\boldsymbol{\beta}_*, \boldsymbol{\beta}_*) - \mathbf{k}_t(\boldsymbol{\beta}_*)^T (\mathbf{K}_t + \sigma_f^2 \mathbf{I})^{-1} \mathbf{k}_t(\boldsymbol{\beta}_*) \quad (16)$$

where $\mathbf{k}_t(\boldsymbol{\beta}) = [k(\mathbf{x}_0, \boldsymbol{\beta}), \dots, k(\mathbf{x}_t, \boldsymbol{\beta})]^T$ and $\mathbf{K}_t = [k(\mathbf{x}, \mathbf{x}')]_{\mathbf{x}, \mathbf{x}' \in \mathbf{X}_t}$. Using this permutation-invariant, time-varying GP we can select $\boldsymbol{\beta}_{t+1}$ by maximizing a linear combination of the GP posterior mean and variance w.r.t $\boldsymbol{\beta}_t$

$$\boldsymbol{\beta}_{t+1} = \arg \max_{\boldsymbol{\beta}_t} \boldsymbol{\mu}_t(\boldsymbol{\beta}_t) + \sqrt{\kappa_t} \sigma_t(\boldsymbol{\beta}_t), \quad (17)$$

where Eq. (17) is referred to as an *acquisition function* and κ_t is its exploration-exploitation trade-off parameter. We note that there are other acquisition functions available [16, 14, 15]. Our acquisition function, Eq. (17), is the time-varying version of GP-UCB [40, 5], which allows us to obtain convergence results in §4.3 and set κ_t in Theorem 1.

4.2 Ordering Constraints and Permutation Invariance

Recall that the vector $\boldsymbol{\beta} = [\beta_0, \dots, \beta_{d-1}]^T$ holds the locations of the left Riemann integral approximation in Eq. (5). In order for the left Riemann approximation to the TVO to be sensible, there must be an ordering constraint imposed on $\boldsymbol{\beta}$ such that $0 < \beta_1 < \dots < \beta_{d-1} < 1$. We model this in our GP using a projection operator Φ which imposes the constraint by sorting the vector $\boldsymbol{\beta}$. Applying Φ within the spatial kernel, we obtain

$$k_\beta(\boldsymbol{\beta}, \boldsymbol{\beta}') := k_S(\Phi(\boldsymbol{\beta}), \Phi(\boldsymbol{\beta}')). \quad (18)$$

This projection does not change the value of our acquisition function, and maintains the positive definite for any covariance function for the spatial k_S , e.g., Matern, Polynomial. We then optimize the acquisition function via a projected-gradient approach. If a $\boldsymbol{\beta}_t$ iterate leaves the feasible set after taking a gradient step, we project it back into the feasible set using Φ and continue. We note that existing work in the GP literature has considered such projection operations in various contexts [38, 43].

4.3 Convergence Analysis

In Eq. (10), we showed that maximizing the TVO objective function $\mathcal{L}_{\mathcal{T}}$ as a function of $\boldsymbol{\beta}_t$ is equivalent to minimizing the cumulative regret $R_{T/w}$ by sequential optimization within the bandit framework. Here, the subscript T/w refers to the number of bandit updates given the maximum epochs T and the update frequency w where $w \ll T$.

We now derive an upper bound on the cumulative regret, and show that it asymptotically goes to zero as T increases, i.e., $\lim_{T \rightarrow \infty} \frac{R_{T/w}}{T} = 0$. Thus, our bandit will converge to choosing $\boldsymbol{\beta}_T$ which yields the optimal value of the TVO objective $\mathcal{L}_{\mathcal{T}}^*$ for model parameters at step T .

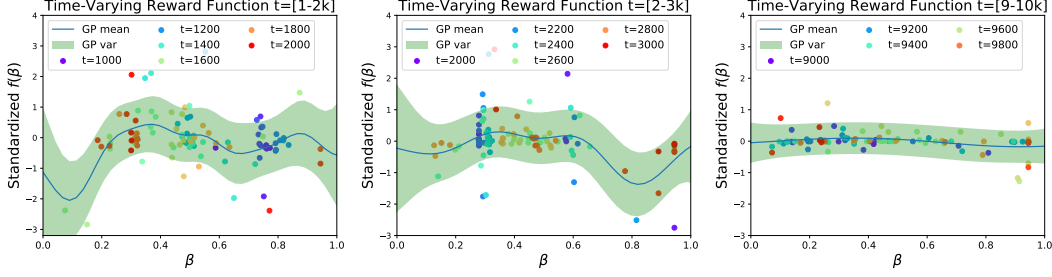


Figure 2: Time-varying reward function $f_t(\beta_t)$ after 2k, 3k, and 10k training epochs, with bandit choices of a single intermediate β_1 (i.e. $\beta = [0, \beta_1]$) colored by timestep. Scattered β_1 in neighboring epochs indicate ‘exploration’, while similarly colored values of β_1 in regions where the GP mean, or predicted reward, is high indicate ‘exploitation’.

We present the main theoretical result in Theorem 1. Our TVO framework mirrors the standard time-varying GP bandit optimization, and thus inherits convergence guarantees from Bogunovic et al. [5]. However, as discussed in Appendix §C, we provide a tighter bound on the mutual information gain $\gamma_{T/w}$ which may be of wider interest.

Theorem 1. *Let the domain $\mathcal{D} \subset [0, 1]^d$ be compact and convex. Let $L_t \geq 0$ be the Lipschitz constant for the reward function at time t . Assume that the covariance function k is almost surely continuously differentiable, with $f \sim GP(0, k)$. Further, for $t \leq T$ and $j \leq d$, we assume*

$$\Pr\left(\sup\left|\partial f_t(\beta_t)/\partial \beta_t^{(j)}\right| \geq L_t\right) \leq ae^{-(L_t/b)^2}$$

for appropriate choice of a and b corresponding to L_t .

For $\delta \in (0, 1)$, we write $\kappa_{T/w} = 2 \log \frac{\pi^2 T^2}{2\delta w^2} + 2d \log db \frac{T^2}{w^2} \sqrt{\log \frac{da\pi^2 T^2}{2\delta w^2}}$ and $C_1 = 8/\log(1 + \sigma_f^2)$. Then, after T/w time steps, our algorithm satisfies

$$R_{T/w} = \sum_{t=1}^{T/w} f_t(\beta_t^*) - f_t(\beta_t) \leq \sqrt{\gamma_{T/w} \cdot C_1 \cdot \kappa_{T/w} \cdot T/w} + 2$$

with probability at least $1 - \delta$, where $\gamma_{T/w}$ is the maximum information gain for the time-varying covariance function (see below).

In the above theorem, the quantity $\gamma_{T/w}$ measures the maximum information gain obtained about the reward function after pulling T/w arms [40, 5]. In the Appendix §C, we show that $\gamma_{T/w} \leq \left(1 + T/[w\tilde{N}]\right) \left(\gamma_{\tilde{N}}^\beta + \sigma_f^{-2}\tilde{N}^{5/2}\omega\right)$, where $\tilde{N} \in \{1, \dots, T/w\}$ denotes a time-varying block length, and $\gamma_{\tilde{N}}^\beta$ is defined with respect to the covariance kernel for β . For our particular choice of exponentiated-quadratic kernel, the maximum information gain scales as $\gamma_{\tilde{N}}^\beta \leq \mathcal{O}(\log \tilde{N}^{d+1})$ [40]. Compared with [5], our proof tightens the upper bound on $\gamma_{T/w}$ from $\mathcal{O}(\tilde{N}^3)$ to $\mathcal{O}(\tilde{N}^{5/2})$.

Combining these terms, we can then write the bound as $R_{T/w} \lesssim \mathcal{O}\left(\sqrt{\left(\log \tilde{N}^{d+1} + \sigma_f^{-2}\tilde{N}^{5/2}\omega\right) T/w}\right)$, which is sublinear in T when the function f becomes time-invariant, i.e., $\omega \rightarrow 0$. In contrast, the sublinear guarantee does not hold when the time-varying function is non-correlated, i.e., $\omega = 1$, in which case the time covariance matrix becomes identity matrix. The bound is tighter for lower schedule dimension d .

5 Experiments

We demonstrate the effectiveness of our method for training VAEs [18] on MNIST and Fashion MNIST, and a Sigmoid Belief Network [28] on binarized MNIST and binarized Omniglot, using the TVO objective. In Appendix D, we explore learning and inference in a discrete probabilistic context-free grammar [24], showing that the TVO objective and our bandit optimization can translate to other

learning settings. In addition, we run ablation studies using random choices of β and a GP without permutation invariance, and compare the runtime and performance of our method with grid search. Our code is available at http://github.com/ntienvu/tvo_gp_bandit.

Experimental Setup: We evaluate our GP-bandit for $S \in \{10, 50\}$ and $d \in \{2, 5, 10, 15\}$ and, for each configuration, train until convergence using 5 random seeds. Note that, for each setting of d , we implicitly include $\beta_0 = 0$ and append 1 to the vector β to perform the integration in Eq. (5).

For each S, d configuration, we compare against three baseline integration schedules: log-uniform spacing in the interval $[\beta_1, 1]$, linear-uniform spacing in the interval $[0, 1]$, and the moments schedule of [6, 12], which corresponds to uniform spacing along the y-axis. For log/linear-uniform spacing, we set $\beta_1 = 0.025$ for all experiments, reflecting the results of grid search in [27]. We use a fixed model architecture for all experiments, which we describe in Appendix A.

To obtain the bandit feedback in Eq. (7), we use a fixed, linear schedule with $d = 50$ for calculating \mathcal{L}_t with Eq. (5). This yields a tighter $\log p_\theta(\mathbf{x})$ bound, decouples reward function evaluation from model training and schedule selection in each round, and is still efficient using SNIS in Eq. (4). We limit the value of d for TVO training following observations of deteriorating performance in [27].

GP Implementation: For GP modeling, we use an exponentiated quadratic covariance function for k_β and estimate hyperparameters via type II maximum likelihood estimation [34]. We use multi-start BFGS [9] to optimize the acquisition function in Eq. (17). We set the update frequency $w = 6$ initially and increment w by one after every 10 bandit iterations to account for smaller objective changes later in training, and update early if $\mathcal{L}_t \leq -0.05$. We found that selecting β_j too close to either 0 or 1 could negatively affect performance, and thus restrict $\beta \in [0.05, 0.95]^d$ in all experiments. We follow a common practice to standardize with the running average the utility score $y \sim \mathcal{N}(0, 1)$ for robustness.

5.1 Scheduling Behaviour

We first investigate the behaviour of our time-varying reward function and bandit scheduling. These experiments highlight the adaptive nature of our algorithm, as we inspect the choice of integration schedule across training epochs for both $d = 2$ and $d = 5$.

Time-varying Reward Function: In Figure 2, we visualize the mean and variance of our time-varying estimate of the utility function $y_t = f_t(\beta_t) + \epsilon_t$ after 2000, 3000, and 10,000 epochs, respectively. We illustrate the choice of β for $d = 2$, so that $\beta_0 = 0$ is fixed and we can write the reward as $f_t(\beta_1)$. Colored dots indicate values of β_1 selected by our bandit algorithm in each round, with the vertical axis reflecting the observed reward $f_t(\beta_1)$ as the change in model evidence \mathcal{L} .

In the first two panels, we observe instances where our bandit prioritizes exploitation, choosing similar, high-reward β_1 values in neighboring rounds with the same color. However, note that these β_1 may not match the highest GP predictive mean for $f_t(\beta)$, since the blue line is shown at the final training epoch in a window. In the final panel, we observe that our time-varying reward function has adapted to have very low variance, since the TVO objective changes only slightly near convergence and the choice of β_1 has little impact.

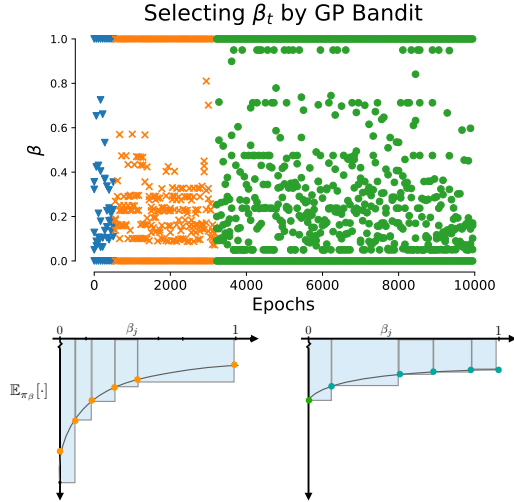


Figure 3: Bandit-chosen β over time on MNIST using $d = 5$. We can interpret the β selection process in 3 phases: (blue) random selection in initial epochs; (orange) focusing on small values $\beta_i < 0.5$ as training progresses; (green) moving toward $\beta_i = 1$ as learning approaches convergence. The bottom panel illustrates a hypothetical integrand curve and β selections at intermediate (left) and later (right) epochs.

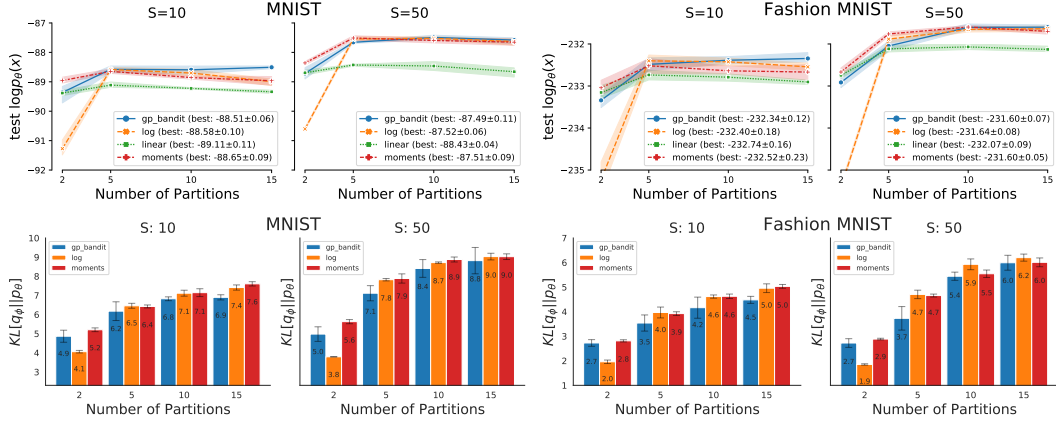


Figure 4: Performance comparison for continuous VAE on MNIST and Fashion MNIST. *Top:* we compare model learning performance using test likelihood (higher is better). *Bottom:* We compare posterior inference as measured by the test KL divergence (lower is better) against the log and moments baselines. Although, in general, we find that models with worse $\log p(\mathbf{x})$ tend to have lower D_{KL} , our GP-bandit schedule provides improvements in both learning and inference.

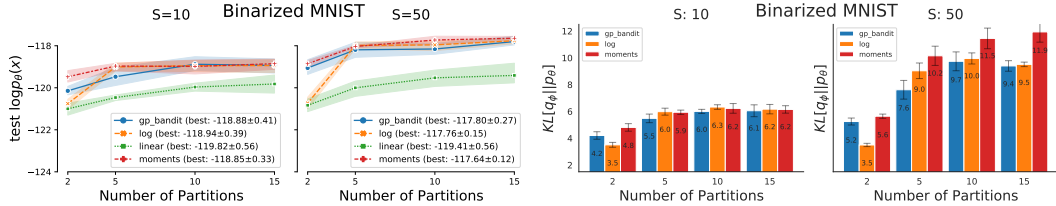


Figure 5: Performance comparison in discrete latent variable model using a Sigmoid Belief Network on the binarized MNIST dataset. Our GP-bandit achieves comparable results to the log and moments schedule in terms model learning (higher $\log p(\mathbf{x})$), with better posterior inference (lower D_{KL}).

β Across Training: In Figure 3, we visualize bandit choices of β with $d = 5$. In initial epochs (blue), the GP-bandit algorithm prioritizes exploration before focusing on $\beta_j < 0.5$ in the second phase (orange). As the VAE converges, our algorithm begins to explore β_j further from zero (green).

Beyond avoiding the need for an expensive grid search, a primary motivation for our bandit approach is a lack of knowledge about the shape of the integrand. Using the intuition that β_j choices should be concentrated in regions where the integrand is changing quickly in order to obtain accurate Riemann approximations, we can still translate the observed bandit choices of β into example integrands in the middle (orange) and late (green) stages of training in the bottom panel of Fig. 3. An integrand that rises steeply away from $\beta = 0$ indicates that $q_\phi(\mathbf{z} | \mathbf{x})$ is mismatched to $p_\theta(\mathbf{z} | \mathbf{x})$, and the TVO might be improved by choosing small β_j . As the curve begins to smooth later in training, with a higher proportion of importance samples yielding high likelihood under the generative model, our bandit begins to explore β_j closer to 1.

5.2 Model Learning and Inference

Continuous VAE: We present results of training a continuous VAE on the MNIST and Fashion MNIST dataset in Figure 4. We measure model learning performance using the test log evidence, as estimated by the IWAE bound [7] with 5000 samples per data point. We also compare inference performance using $D_{KL}[q_\phi(\mathbf{z} | \mathbf{x}) || p_\theta(\mathbf{z} | \mathbf{x})]$, which we calculate by subtracting the test ELBO from our estimate of $\log p_\theta(\mathbf{x})$.

For most scenarios in Figure 4, our GP bandit optimization outperforms baselines with respect to both model learning and inference. In general, we observe that models with lower model evidence attain lower test KL divergence. Thus, in comparing inference performance in the bottom panel of Figure 4, we compare against the log and moment schedules, baselines with comparable test log

likelihoods. It is notable that our approach often achieves better results for both learning (higher $\log p_\theta(\mathbf{x})$) and inference (lower D_{KL}). We obtain the highest log evidence with $d = 10$ for MNIST and $d = 15$ for Fashion MNIST.

Sigmoid Belief Network: We present similar results for learning discrete latent variable models using a Sigmoid Belief Network [28]. We show results on binarized MNIST in Figure 5, with binarized Omniglot in Figure 7 in Appendix D.2. Our GP bandit optimization achieves competitive model learning performance with the log-uniform and moment schedules and better posterior inference across models with comparable $\log p(\mathbf{x})$, indicating our GP-bandit schedule can flexibly optimize the TVO for various model types.

6 Conclusion

We have presented a new approach for automated selection of the integration schedule for the Thermodynamic Variational Objective. Our bandit framework optimizes a reward function that is directly linked to improvements in the generative model evidence over the course of training the model parameters. We show theoretically that this procedure asymptotically minimizes the regret as a function of the choice of schedule. Finally, we demonstrated that the proposed approach empirically outperforms existing schedules in both model learning and inference for discrete and continuous generative models.

Our GP bandit optimization offers a general solution to choosing the integration schedule in the TVO. However, our algorithm, as well as all other existing schedules, still rely on the number of partitions d as a hyperparameter which is fixed over the course of the training. Incorporating the adaptive selection of d into our bandit optimization remains an interesting direction for future work.

7 Broader Impact

Our research can be widely applied for variational inference in deep generative models, including variational autoencoders with autoregressive decoders and normalizing flows. Variational inference, and Bayesian methods more generally, have broad applications spanning science and engineering, from epidemiology [45] to particle physics [2]. Our methodological contributions for variational inference may find broader impact through improved modelling in these disparate domains. However, our method is general in nature, so domain-specific applications should further consider implications for deployment in the real-world.

8 Acknowledgements

VM acknowledges the support of the Natural Sciences and Engineering Research Council of Canada (NSERC) under award number PGSD3-535575-2019 and the British Columbia Graduate Scholarship, award number 6768. VM/FW acknowledge the support of the Natural Sciences and Engineering Research Council of Canada (NSERC), the Canada CIFAR AI Chairs Program, and the Intel Parallel Computing Centers program. RB acknowledges support from the Defense Advanced Research Projects Agency (DARPA) under award FA8750-17-C-0106.

This material is based upon work supported by the United States Air Force Research Laboratory (AFRL) under the Defense Advanced Research Projects Agency (DARPA) Data Driven Discovery Models (D3M) program (Contract No. FA8750-19-2-0222) and Learning with Less Labels (LwLL) program (Contract No. FA875019C0515). Additional support was provided by UBC’s Composites Research Network (CRN), Data Science Institute (DSI) and Support for Teams to Advance Interdisciplinary Research (STAIR) Grants. This research was enabled in part by technical support and computational resources provided by WestGrid (<https://www.westgrid.ca/>) and Compute Canada (www.computecanada.ca).

References

- [1] Peter Auer, Nicolo Cesa-Bianchi, Yoav Freund, and Robert E Schapire. The nonstochastic multiarmed bandit problem. *SIAM journal on computing*, 32(1):48–77, 2002.

- [2] Atilim Gunes Baydin, Lei Shao, Wahid Bhimji, Lukas Heinrich, Saeid Naderiparizi, Andreas Munk, Jialin Liu, Bradley Gram-Hansen, Gilles Louppe, Lawrence Meadows, et al. Efficient probabilistic inference in the quest for physics beyond the standard model. In *Advances in Neural Information Processing Systems*, pages 5460–5473, 2019.
- [3] Christopher M Bishop. *Pattern recognition and machine learning*. springer New York, 2006.
- [4] David M Blei, Alp Kucukelbir, and Jon D McAuliffe. Variational inference: A review for statisticians. *Journal of the American statistical Association*, 112(518):859–877, 2017.
- [5] Ilija Bogunovic, Jonathan Scarlett, and Volkan Cevher. Time-varying Gaussian process bandit optimization. In *Artificial Intelligence and Statistics*, pages 314–323, 2016.
- [6] Rob Brekelmans, Vaden Masrani, Frank Wood, Greg Ver Steeg, and Aram Galstyan. All in the exponential family: Bregman duality in thermodynamic variational inference. In *International Conference on Machine Learning*, 2020.
- [7] Yuri Burda, Roger Grosse, and Ruslan Salakhutdinov. Importance weighted autoencoders. In *International Conference on Representation Learning*, 2016.
- [8] Chris Cremer, Xuechen Li, and David Duvenaud. Inference suboptimality in variational autoencoders. In *International Conference on Machine Learning*, pages 1078–1086, 2018.
- [9] Roger Fletcher. *Practical methods of optimization*. John Wiley & Sons, 2013.
- [10] Daan Frenkel and Berend Smit. *Understanding molecular simulation: from algorithms to applications*, volume 1. Elsevier, 2001.
- [11] Andrew Gelman and Xiao-Li Meng. Simulating normalizing constants: From importance sampling to bridge sampling to path sampling. *Statistical science*, pages 163–185, 1998.
- [12] Roger B Grosse, Chris J Maddison, and Russ R Salakhutdinov. Annealing between distributions by averaging moments. In *Advances in Neural Information Processing Systems*, pages 2769–2777, 2013.
- [13] Junxian He, Daniel Spokoyny, Graham Neubig, and Taylor Berg-Kirkpatrick. Lagging inference networks and posterior collapse in variational autoencoders. In *International Conference on Representation Learning*, 2019.
- [14] Philipp Hennig and Christian J Schuler. Entropy search for information-efficient global optimization. *Journal of Machine Learning Research*, 13:1809–1837, 2012.
- [15] José Miguel Hernández-Lobato, Matthew W Hoffman, and Zoubin Ghahramani. Predictive entropy search for efficient global optimization of black-box functions. In *Advances in Neural Information Processing Systems*, pages 918–926, 2014.
- [16] Donald R Jones, Matthias Schonlau, and William J Welch. Efficient global optimization of expensive black-box functions. *Journal of Global optimization*, 13(4):455–492, 1998.
- [17] Diederik P Kingma and Jimmy Ba. Adam: A method for stochastic optimization. *International Conference on Learning Representations*, 2014.
- [18] Diederik P. Kingma and Max Welling. Auto-encoding variational bayes. In *International Conference on Learning Representations*, 2014.
- [19] Durk P Kingma, Tim Salimans, Rafal Jozefowicz, Xi Chen, Ilya Sutskever, and Max Welling. Improved variational inference with inverse autoregressive flow. In *Advances in Neural Information Processing Systems*, pages 4743–4751, 2016.
- [20] Aaron Klein, Stefan Falkner, Simon Bartels, Philipp Hennig, and Frank Hutter. Fast Bayesian optimization of machine learning hyperparameters on large datasets. In *Artificial Intelligence and Statistics*, pages 528–536, 2017.
- [21] Andreas Krause and Cheng S Ong. Contextual Gaussian process bandit optimization. In *Advances in Neural Information Processing Systems*, pages 2447–2455, 2011.

- [22] Brenden M Lake, Russ R Salakhutdinov, and Josh Tenenbaum. One-shot learning by inverting a compositional causal process. In *Advances in Neural Information Processing Systems*, pages 2526–2534, 2013.
- [23] Brenden M Lake, Ruslan Salakhutdinov, and Joshua B Tenenbaum. Human-level concept learning through probabilistic program induction. *Science*, 350(6266):1332–1338, 2015.
- [24] Tuan Anh Le, Adam R Kosior, N Siddharth, Yee Whye Teh, and Frank Wood. Revisiting reweighted wake-sleep for models with stochastic control flow. In *Uncertainty in Artificial Intelligence*, pages 1039–1049. PMLR, 2020.
- [25] Yann LeCun, Léon Bottou, Yoshua Bengio, and Patrick Haffner. Gradient-based learning applied to document recognition. *Proceedings of the IEEE*, 86(11):2278–2324, 1998.
- [26] Yucen Luo, Alex Beatson, Mohammad Norouzi, Jun Zhu, David Duvenaud, Ryan P Adams, and Ricky TQ Chen. Sumo: Unbiased estimation of log marginal probability for latent variable models. *arXiv preprint arXiv:2004.00353*, 2020.
- [27] Vaden Masrani, Tuan Anh Le, and Frank Wood. The thermodynamic variational objective. In *Advances in Neural Information Processing Systems*, pages 11521–11530, 2019.
- [28] Andriy Mnih and Karol Gregor. Neural variational inference and learning in belief networks. In *International Conference on Machine Learning*, pages 1791–1799, 2014.
- [29] Andriy Mnih and Danilo J Rezende. Variational inference for monte carlo objectives. In *International Conference on Machine Learning*, pages 2188–2196, 2016.
- [30] Vu Nguyen, Sebastian Schulze, and Michael A Osborne. Bayesian optimization for iterative learning. In *Advances in Neural Information Processing Systems*, 2020.
- [31] Sebastian Nowozin. Debiasing evidence approximations: On importance-weighted autoencoders and jackknife variational inference. *International Conference on Learning Representations*, 2018.
- [32] Favour Mandanji Nyikosa. *Adaptive Bayesian optimization for dynamic problems*. PhD thesis, University of Oxford, 2018.
- [33] Yosihiko Ogata. A monte carlo method for high dimensional integration. *Numerische Mathematik*, 55(2):137–157, 1989.
- [34] Carl Edward Rasmussen. *Gaussian processes for machine learning*. 2006.
- [35] Danilo Rezende and Shakir Mohamed. Variational inference with normalizing flows. In *International Conference on Machine Learning*, pages 1530–1538, 2015.
- [36] Danilo Jimenez Rezende, Shakir Mohamed, and Daan Wierstra. Stochastic backpropagation and approximate inference in deep generative models. In *International Conference on Machine Learning*, pages 1278–1286, 2014.
- [37] Ruslan Salakhutdinov and Iain Murray. On the quantitative analysis of deep belief networks. In *International Conference on Machine Learning*, pages 872–879, 2008.
- [38] Jasper Snoek, Kevin Swersky, Rich Zemel, and Ryan Adams. Input warping for Bayesian optimization of non-stationary functions. In *International Conference on Machine Learning*, pages 1674–1682, 2014.
- [39] Casper Kaae Sønderby, Tapani Raiko, Lars Maaløe, Søren Kaae Sønderby, and Ole Winther. Ladder variational autoencoders. In *Advances in Neural Information Processing Systems 29*, pages 3738–3746. 2016.
- [40] Niranjan Srinivas, Andreas Krause, Sham Kakade, and Matthias Seeger. Gaussian process optimization in the bandit setting: No regret and experimental design. In *International Conference on Machine Learning*, pages 1015–1022, 2010.

- [41] Kevin Swersky, Jasper Snoek, and Ryan P Adams. Multi-task Bayesian optimization. In *Advances in Neural Information Processing Systems*, pages 2004–2012, 2013.
- [42] Michael Tschannen, Olivier Bachem, and Mario Lucic. Recent advances in autoencoder-based representation learning. *arXiv preprint arXiv:1812.05069*, 2018.
- [43] Mark van der Wilk, Matthias Bauer, ST John, and James Hensman. Learning invariances using the marginal likelihood. In *Advances in Neural Information Processing Systems*, pages 9938–9948, 2018.
- [44] Martin J Wainwright and Michael I Jordan. Graphical models, exponential families, and variational inference. *Foundations and Trends® in Machine Learning*, 1(1-2):1–305, 2008.
- [45] Frank Wood, Andrew Warrington, Saeid Naderiparizi, Christian Weilbach, Vaden Masrani, William Harvey, Adam Scibior, Boyan Beronov, and Ali Nasser. Planning as inference in epidemiological models. *arXiv preprint arXiv:2003.13221*, 2020.
- [46] Han Xiao, Kashif Rasul, and Roland Vollgraf. Fashion-mnist: a novel image dataset for benchmarking machine learning algorithms. *arXiv preprint arXiv:1708.07747*, 2017.

A Experimental Setup

Dataset Description The discrete and continuous VAE literature use slightly different training procedures. For continuous VAEs, we follow the sampling procedure described in footnote 2, page 6 of Burda et al. [7], and sample binary-valued pixels with expectation equal to the original gray scale 28×28 image. We split MNIST [25] and Fashion MNIST [46] into 60k training examples and 10k testing examples across 10 classes.

For Sigmoid Belief Networks, we follow the procedure described by Mnih and Rezende [29] and use 50k training examples and 10k testing examples (the remaining 10k validation examples are not used) with the binarized MNIST [37] dataset.

Training Procedure All models are written in PyTorch and trained on GPUs. For each scheduler, we train for 10,000 epochs using the Adam optimizer [17] with a learning rate of 10^{-3} , and minibatch size of 1000. All weights are initialized with PyTorch’s default initializer. For the neural network architecture, we use two hidden layers of [100, 25] nodes.

Reward Evaluation To obtain the bandit feedback in Eq. (7), we use a fixed, linear schedule with $d = 50$ for calculating \mathcal{L}_t with Eq. (5). This yields a tighter $\log p_\theta(\mathbf{x})$ bound, decouples reward function evaluation from model training and schedule selection in each round, and is still efficient using SNIS in Eq. (4). We limit the value of d for TVO training following observations of deteriorating performance in [27].

B GP kernels and treatment of GP hyperparameters

We present the GP kernels and treatment of GP hyperparameters for the black-box function f .

We use the exponentiated quadratic (or squared exponential) covariance function for input hyperparameter $k_\beta(\boldsymbol{\beta}, \boldsymbol{\beta}') = \exp\left(-\frac{\|\boldsymbol{\beta} - \boldsymbol{\beta}'\|^2}{2\sigma_\beta^2}\right)$ and a time kernel $k_T(t, t') = (1 - \omega)^{\frac{|t - t'|}{2}}$ where the observation $\boldsymbol{\beta}$ and t are normalized to $[0, 1]^d$ and the outcome y is standardized $y \sim \mathcal{N}(0, 1)$ for robustness. As a result, our product kernel becomes

$$k([\boldsymbol{\beta}, t], [\boldsymbol{\beta}', t']) = k(\boldsymbol{\beta}, \boldsymbol{\beta}') \times k(t, t') = \exp\left(-\frac{\|\boldsymbol{\beta} - \boldsymbol{\beta}'\|^2}{2\sigma_\beta^2}\right) (1 - \omega)^{\frac{|t - t'|}{2}}.$$

The length-scales σ_β is estimated from the data indicating the variability of the function with regards to the hyperparameter input \mathbf{x} and number of training iterations t . Estimating appropriate values for them is critical as this represents the GP’s prior regarding the sensitivity of performance w.r.t. changes in the number of training iterations and hyperparameters. We note that previous works have also utilized the above product of spatial and temporal covariance functions for different settings [21, 5, 30].

We fit the GP hyperparameters by maximizing their posterior probability (MAP), $p(\sigma_l, \omega \mid \boldsymbol{\beta}, \mathbf{t}, \mathbf{y}) \propto p(\sigma_l, \omega, \boldsymbol{\beta}, \mathbf{t}, \mathbf{y})$, which, thanks to the Gaussian likelihood, is available in closed form as [34]

$$\ln p(\mathbf{y}, \boldsymbol{\beta}, \mathbf{t}, \sigma_l, \omega) = \frac{1}{2} \mathbf{y}^T (\mathbf{K} + \sigma^2 \mathbf{I}_N)^{-1} \mathbf{y} - \frac{1}{2} \ln |\mathbf{K} + \sigma^2 \mathbf{I}_N| + \ln p_{\text{hyp}}(\sigma_x, \omega) + \text{const} \quad (19)$$

where \mathbf{I}_N is the identity matrix in dimension N (the number of points in the training set), and $p_{\text{hyp}}(\sigma_l, \omega)$ is the prior over hyperparameters, described in the following.

We maximize the marginal likelihood in Eq. (19) to select the suitable lengthscale parameter σ_l , remembering-forgetting trade-off ω , and noise variance σ_f^2 .

Optimizing Eq. (19) involves taking the derivative w.r.t. each variable, such as $\frac{\partial \ln p(\mathbf{y}, \boldsymbol{\beta}, \mathbf{t}, \sigma_l, \omega)}{\partial \omega} = \frac{\partial \ln p(\mathbf{y}, \boldsymbol{\beta}, \mathbf{t}, \sigma_l, \omega)}{\partial \mathbf{K}} \times \frac{\partial \mathbf{K}}{\partial k(t, t')} \times \frac{\partial k(t, t')}{\partial \omega}$. While the derivatives of σ_l and σ_f^2 are standard and can be found in [34], we present the derivative w.r.t. ω as follows

$$\frac{\partial k(t, t')}{\partial \omega} = -v (1 - \omega)^{v-1} \text{ where } v = |t - t'|/2. \quad (20)$$

We optimize Eq. (19) with a gradient-based optimizer, providing the analytical gradient to the algorithm. We start the optimization from the previous hyperparameter values θ_{prev} . If the optimization fails due to numerical issues, we keep the previous value of the hyperparameters.

C Proof of Theorem 1

Our use of the TVGP within the TVO setting requires no problem specific modifications compared to the general formulation in Bogunovic. As such, the proof of Theorem 1 closely follows the proof of Theorem 4.3 in Bogunovic et al. [5] App. C. with time kernel $k_T(i, j) = (1 - \omega)^{\frac{|i-j|}{2}}$. At a high level, their proof proceeds by partitioning the T random functions into blocks of length \tilde{N} , and bounding each using Mirsky’s theorem. Referring to Table 1 for notation, this results in a bound on the maximum mutual information

$$\tilde{\gamma}_{\tilde{N}} \leq \left(\frac{T}{\tilde{N}} + 1\right) (\gamma_{\tilde{N}} + \tilde{N}^3 \omega), \quad (21)$$

which leads directly to their bound on the cumulative regret (cf. App C.2 in [5]). Our contribution is to recognize we can achieve a tighter bound on the maximum mutual information with an application Cauchy Schwarz and Jensen’s inequality.

Proof. Beginning from Bogunovic et al. [5] Eq. (58), we have

$$\tilde{\gamma}_{\tilde{N}} \leq \gamma_{\tilde{N}} + \sum_{i=1}^{\tilde{N}} \log(1 + \Delta_i) \quad (22)$$

$$\tilde{\gamma}_{\tilde{N}} \leq \gamma_{\tilde{N}} + \tilde{N} \log \left(1 + \frac{1}{\tilde{N}} \sum_{i=1}^{\tilde{N}} \Delta_i \right) \quad \text{Jensen’s inequality} \quad (23)$$

$$\tilde{\gamma}_{\tilde{N}} \leq \gamma_{\tilde{N}} + \tilde{N} \log \left(1 + \frac{1}{\sqrt{\tilde{N}}} \sqrt{\sum_{i=1}^{\tilde{N}} \Delta_i^2} \right) \quad \text{Cauchy-Schwartz} \quad (24)$$

$$\tilde{\gamma}_{\tilde{N}} \leq \gamma_{\tilde{N}} + \tilde{N} \log \left(1 + \tilde{N}^{3/2} \omega \right) \quad \sum_{i=1}^{\tilde{N}} \Delta_i^2 \leq \tilde{N}^4 \omega^2 \quad (25)$$

$$\tilde{\gamma}_{\tilde{N}} \leq \gamma_{\tilde{N}} + \tilde{N}^{5/2} \omega \quad \log(1 + x) \leq x \quad (26)$$

This bound is tighter than [5] Eq. (60) ($\tilde{N}^{5/2} \leq \tilde{N}^3$), where the latter was achieved via a simple constrained optimization argument. Using (26), Theorem 1 follows using identical arguments as in [5]. \square

D Additional Experiments and Ablation Studies

We present additional experiments on a Probabilistic Context Free Grammar (PCFG) model and Sigmoid Belief Networks in §D.1 and §D.2, a wall-clock time benchmark in §D.3, ablation studies in §D.4, and additional training curves in §D.5.

D.1 Training Probabilistic Context Free Grammar

In order to evaluate our method outside of the Variational Autoencoder framework, we consider model learning and amortized inference in the probabilistic context-free grammar setting described in Section 4.1 of Le et al. [24]. Here $p_\theta(\mathbf{x}, \mathbf{z}) = p(\mathbf{x} | \mathbf{z}) p_\theta(\mathbf{z})$, where $p_\theta(\mathbf{z})$ is a prior over parse trees \mathbf{z} , $p(\mathbf{x} | \mathbf{z})$ is a soft relaxation of the $\{0, 1\}$ likelihood which indicates if sentence \mathbf{x} matches the set of terminals (i.e the sentence) produced by \mathbf{z} , and θ is the set of probabilities associated with each production rule in the grammar. The inference network ϕ is a recurrent neural network which outputs $q_\phi(\mathbf{z} | \mathbf{x})$, the conditional distribution of a parse tree given an input sentence. We use

Table 1: Supporting notations in regret analysis. We use notation to similar to Appendix C of Bogunovic et al. [5] when possible.

Parameter	Domain	Meaning
ω	scalar, $(0, 1)$	Remembering-forgetting trade-off parameter (ϵ in [5])
\mathbf{f}_T	vector, \mathbb{R}^T	Vector of T function evaluations from f , $\mathbf{f}_T := [f(x_1), \dots, f(x_T)]^T$.
$\tilde{\mathbf{f}}_T$	vector, \mathbb{R}^T	(<i>time-varying case</i>) Vector of T function evaluations from $f_{1:T}$, $\tilde{\mathbf{f}}_T := [f_1(x_1), \dots, f_T(x_T)]^T$
$I(\mathbf{y}_T; \mathbf{f}_T)$	scalar, \mathbb{R}^+	The mutual information in \mathbf{f}_T after revealing $\mathbf{y}_T = \mathbf{f}_T + \epsilon$. For a GP with covariance function \mathbf{K}_T , $I(\mathbf{y}_T; \mathbf{f}_T) = \frac{1}{2} \log \mathbf{I} + \sigma^{-2} \mathbf{K}_T $
$\tilde{I}(\mathbf{y}_T; \tilde{\mathbf{f}}_T)$	scalar, \mathbb{R}^+	(<i>time-varying case</i>) Mutual information $\tilde{I}(\mathbf{y}_T; \tilde{\mathbf{f}}_T) = \frac{1}{2} \log \mathbf{I} + \sigma^{-2} \tilde{\mathbf{K}}_T $, where $\tilde{\mathbf{K}}_T$ is a covariance function that incorporates time kernel $k_T(i, j)$
γ_T	scalar, \mathbb{R}^+	The maximum information gain $\gamma_T := \max_{x_1, \dots, x_T} I(\mathbf{y}_T; \mathbf{f}_T)$ after T rounds
$\tilde{\gamma}_T$	scalar, \mathbb{R}^+	(<i>time-varying case</i>) The analogous time-varying maximum information gain $\tilde{\gamma}_T := \max_{x_1, \dots, x_T} \tilde{I}(\mathbf{y}_T; \tilde{\mathbf{f}}_T)$
\tilde{N}	scalar, \mathbb{R}^+	An artifact of the proof technique used by [5]. The T time steps are partitioned into blocks of length \tilde{N}

the *Astronomers* PCFG considered by Le et al. [24], and therefore have access to the ground truth production probabilities θ_{true} , which we will use to evaluate the quality of our learned model θ .

We compare the TVO with GP-bandit and log schedules against REINFORCE, WAKE-WAKE, and WAKE-SLEEP, where WAKE-WAKE and WAKE-SLEEP use data from the true model $\mathbf{x} \sim p_{\theta_{\text{true}}}(\mathbf{x})$ and learned model $\mathbf{x} \sim p_{\theta}(\mathbf{x})$ respectively. For each run, we use a batch size of 2 and train for 2000 epochs with Adam using default parameters. For all KL divergences (see caption in Figure 6), we compute the median over 20 seeds and then plot the average over the last 100 epochs.

As observed by Le et al. [24], sleep- ϕ updates avoid the deleterious effects of the SNIS bias and is therefore preferable to wake- ϕ updates in this context. Therefore for all runs we use the TVO to update θ , and use sleep- ϕ to update ϕ . Sleep- ϕ is a special case of the TVO (cf. Masrani et al. [27] Appendix G.1).

In Figure 6 we see that both GP-bandits and log schedules have comparable performance in this setting, with TVO-log, $S = 20$ achieving the lowest $\text{KL}[p_{\theta} || p_{\theta_{\text{true}}}]$ and $\text{KL}[q_{\phi}(\mathbf{z} | \mathbf{x}) || p_{\theta_{\text{true}}}(\mathbf{z} | \mathbf{x})]$ across all trials. $\text{KL}[q_{\phi} || p_{\theta_{\text{true}}}]$ is a preferable metric to $\text{KL}[q_{\phi} || p_{\theta}]$ because the former does not depend on the quality of the learned model. We also note that GP-bandits appears to be less sensitive to the number of partitions than the log schedule.

D.2 Training Sigmoid Belief Network on Binarized Omniglot

We train the Sigmoid Belief Network described in §5.2 on the binarized Omniglot dataset. Omniglot [22] has 1623 handwritten characters across 50 alphabets. We manually binarize the omniglot[23] dataset by sampling once according to procedure described in [7], and split the binarized omniglot dataset into 23,000 training and 8,070 test examples. Results are shown in Figure 7. At $S = 50$, GP-bandit achieves similar model learning but better inference compared to log scheduling.

D.3 Wall-clock time Comparison

We benchmark the wall-clock time of our GP-bandit schedule against the cumulative wall-clock time of the grid-search log schedule. For both schedules we train a VAE on the Omniglot dataset for $S = 10$ and 5000 epochs. For the log schedule, we run the sweep ran by Masrani et al. [27] (cf. section 7.2), i.e. 20 β_1 linearly spaced between $[10^{-2}, 0.9]$ for $d = 2, \dots, 6$, for a total of 100 runs. For a fair comparison against the log schedule, we loop over $d = 2, \dots, 6$ for our GP bandits because d is unlearned, for a total of five runs. We note that each run of the GP bandits schedule

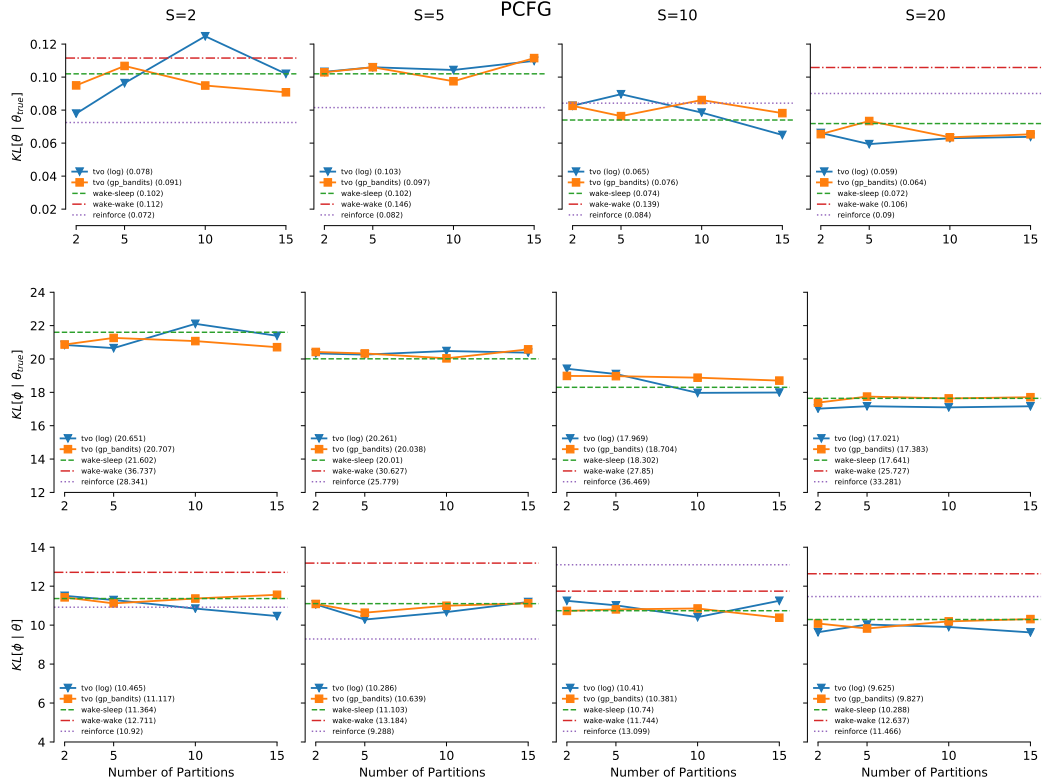


Figure 6: Evaluation of model learning in a PCFG, where θ is the set of probabilities associated with each production rule in the grammar, and ϕ is an RNN which generates the conditional probability of a parse tree given a sentence. GP-bandits (ours) is comparable to the baseline log schedule and less sensitive to number of partitions, as evaluated by the KL divergence between learned and true model parameters (top row). Inference network learning is evaluated by the KL divergence between $q_\phi(\mathbf{z} | \mathbf{x})$ and $p_{\theta_{\text{true}}}(\mathbf{z} | \mathbf{x})$ (middle row) and $p_\theta(\mathbf{z} | \mathbf{x})$ (bottom row). We compare against REINFORCE, WAKE-WAKE, and WAKE-SLEEP, where some baselines aren't shown due to being out of range. At $S = 20$, TVO with log and GP-bandits schedule outperforms REINFORCE, WAKE-WAKE, and WAKE-SLEEP both in terms of the quality of the generative model (top row, right) and inference network (middle row, right) for all $S \in \{2, 5, 10, 20\}$.

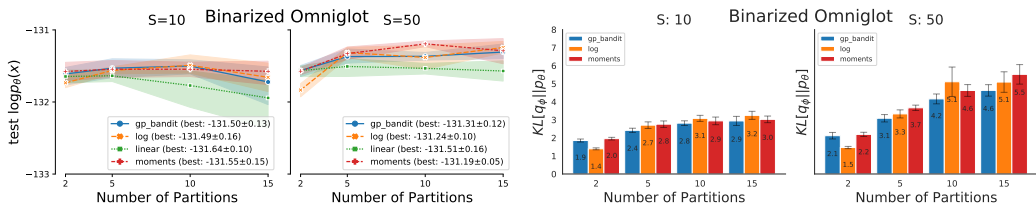


Figure 7: Performance of the Sigmoid Belief Network described in §5.2 on the binarized omniglot dataset. The GP-bandit schedule at $d = 15$, $S = 50$ outperforms all baselines in terms of model and inference network learning.

includes learning the GP hyperparameters as described in Appendix B. For both schedules, we take the best $\log p(x)$ and corresponding KL divergence, and plot the cumulative run time across all runs. The results in Table 2 show that the GP-bandits schedule does comparable to the grid searched log schedule (log likelihood: -110.72 vs -110.99) while requiring significantly less cumulative wall-clock time (10 hrs vs 178 hrs).

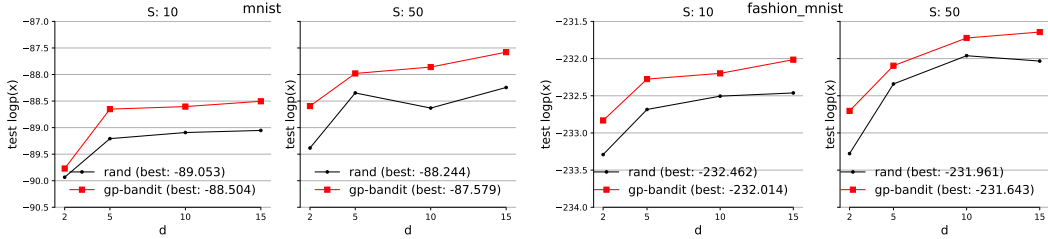


Figure 8: We compare the performance between our GP-bandit against the Random search (Rand) baseline which uniformly generates the integration schedules β_t . The GP-bandit schedule outperforms the random counterpart by using information obtained from previous choices, as described in Algorithm 1.

Table 2: Wallclock time of the GP-bandit schedule compared to the grid-search of [27] for the log schedule. GP-bandit approach achieves a competitive test log likelihood and lower KL divergence compared with the grid-searched log schedule, but requires significantly lower cumulative run-time.

	best log $p(x)$	best kl	number of runs	cumulative run time (hrs)
GP bandit (ours)	-110.995	7.655	5	10.99
grid-searched log	-110.722	8.389	100	177.01

D.4 Ablation studies

Ablation study between GP-bandit and random search. To demonstrate that our model can leverage useful information from past data, we compare against the Random Search picks the integration schedule uniformly at random.

We present the results in Figure 8 using MNIST (left) and Fashion MNIST (right). We observe that our GP-bandit clearly outperforms the Random baseline. The gap is generally increasing with larger dimension d , e.g., $d = 15$ as the search space grows exponentially with the dimension.

Ablation study between permutation invariant GPs. We compare our GP-bandit model using two versions of (1) non-permutation invariant GP and (2) permutation invariant GP in Table 3.

Our permutation invariant GP does not need to add all permuted observations into the model, but is still capable of generalizing. The result in Table 3 confirms that if we have more samples to learn the GP, such as using larger epochs budget T , the two versions will result in the same performance. On the other hand, if we have limited number of training budgets, e.g., using lower number of epochs, the permutation invariant GP will be more favorable and outperforms the non-permutation invariant. In addition, the result suggests that for higher dimension $d = 15$ (number of partitions) our permutation invariant GP performs consistently better than the counterpart.

D.5 Training Curves

We show example training curves for $S = 10, d \in \{5, 15\}$ obtained using the linear, log, moment, and GP-bandit schedules in Figure 9. We can see sudden drops in the GP-bandit training curves indicating our model is exploring alternate schedules during training (cf. Section 4.1).

Table 3: Comparison between permutation invariant and non-permutation invariant in MNIST dataset using S=10 (top) and S=50 (bottom). The best scores are in bold. Given T used epochs, the number of bandit update and thus the number of sample for GP is T/w where $w = 10$ is the frequency update. The permutation invariant will be more favorable when we have less samples for fitting the GP, as indicated in less number of used epochs $T = 1000, 2000$. The performance is comparable when we collect sufficiently large number of samples, e.g., when $T/w = 1000$.

S=10	Used Epoch T / Bandit Iteration	1000/100	2000/200	5000/500	10000/1000
d=5	Perm Invariant	-91.488	-90.129	-89.130	-88.651
	Non Perm Invariant	-91.554	-90.206	-89.262	-88.552
d=10	Perm Invariant	-91.430	-90.219	-89.159	-88.603
	Non Perm Invariant	-91.553	-90.249	-89.110	-88.466
d=15	Perm Invariant	-91.386	-90.059	-88.957	-88.504
	Non Perm Invariant	-91.550	-90.224	-89.215	-88.564
S=50	Used Epoch T / Bandit Iteration	1000/100	2000/200	5000/500	10000/1000
d=5	Permutation Invariant	-90.071	-89.068	-88.163	-87.979
	Non Permutation Invariant	-90.119	-89.142	-88.215	-87.860
d=10	Perm Invariant	-90.125	-89.115	-88.187	-87.859
	Non Permutation Invariant	-90.212	-89.225	-88.231	-87.702
d=15	Permutation Invariant	-90.029	-89.082	-88.102	-87.579
	Non Permutation Invariant	-90.157	-89.247	-88.173	-87.631

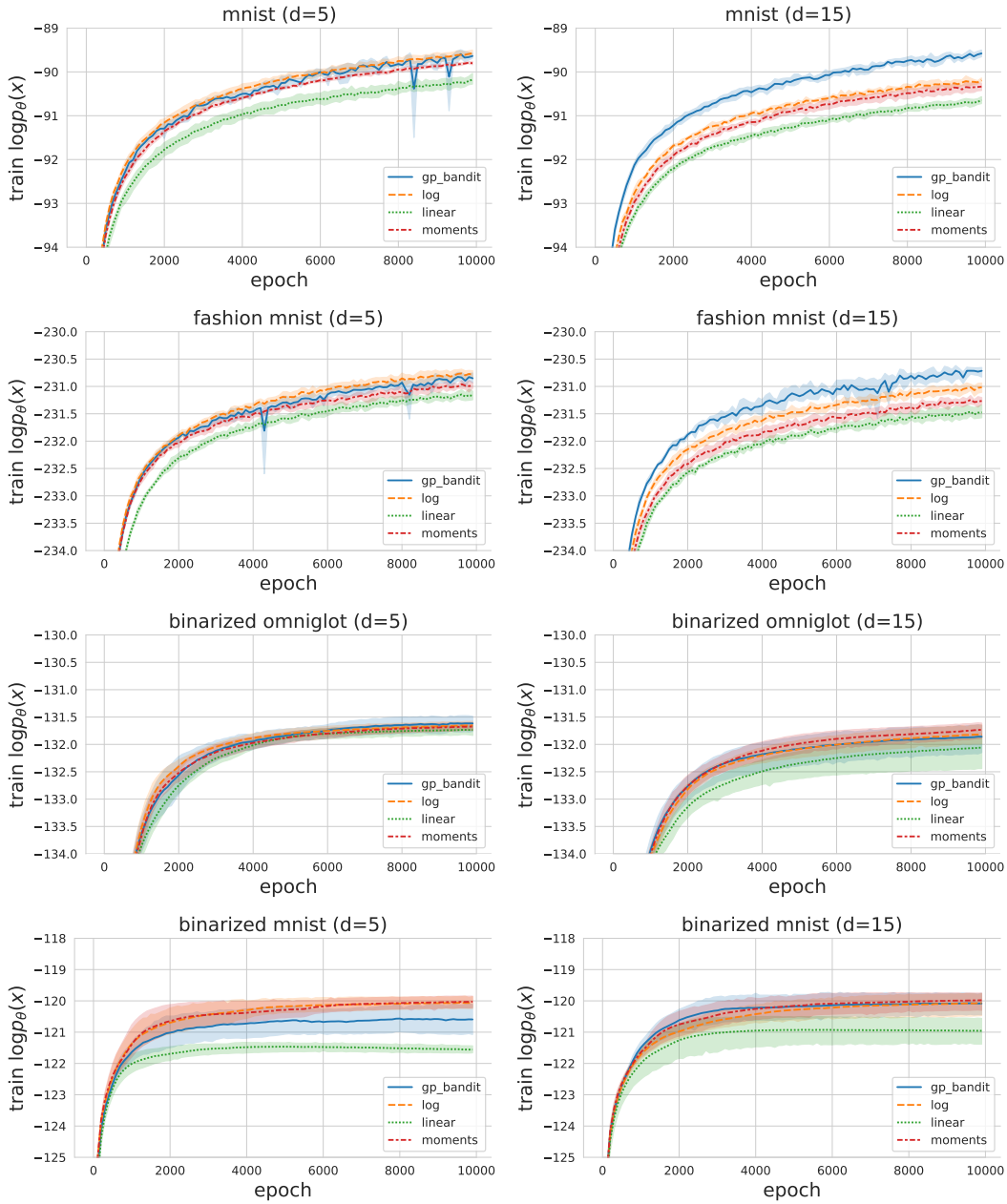


Figure 9: We plot $\log p(x)$ on the training set throughout $S = 10$, $d \in \{5, 15\}$ for each dataset using the experimental setup described in Appendix A. The final training log likelihoods are consistent with the test log likelihoods. Small drops in the GP-bandit training curves indicate the algorithm exploring the reward landscape (see Section 4.1).

1 We thank the reviewers for their insightful comments. We first respond to the common concerns across the four reviews
2 before addressing specific reviewer feedback.

3 **Strength of results, hyperparameters, additional experiments:** All reviewers observe we achieve only modest gains
4 compared to the log-uniform spacing in terms of final log likelihood. We emphasize that while this is true, the main
5 benefit of our approach is in avoiding the costly grid required by the log/linear-uniform spacing schedule. To respond to
6 R4's request, as measured in wall-clock time, our GP-bandit schedule takes approx. 12 hrs to train a VAE on MNIST
7 compared to the approx 160hrs training time for the grid searched log schedule (8 hrs/run x 20 runs). We will update
8 the main text to make these considerations clear, and add an additional appendix section benchmarking our schedule
9 against baselines in terms of total wall-clock time.

10 To respond to R4, all results were obtained from
11 a single seed. We will update the figures in the
12 final draft to average results across five seeds, and
13 have included preliminary results on MNIST in
14 Figure 1. As per R1's request, we will also include
15 the training loss in the final version, which closely
16 mirrors the test loss curves.

17 R2 raises a concern about the number of hyper-
18 parameters in our method. The GP-bandit intro-
19 duces three additional hyperparameters which can
20 be learned directly from data by maximizing the
21 GP marginal likelihood, and therefore require no
22 additional hand-tuning by practitioners as discussed in Appendix B. The exploration-exploitation trade off parameter κ_t
23 is set using Theorem 1.

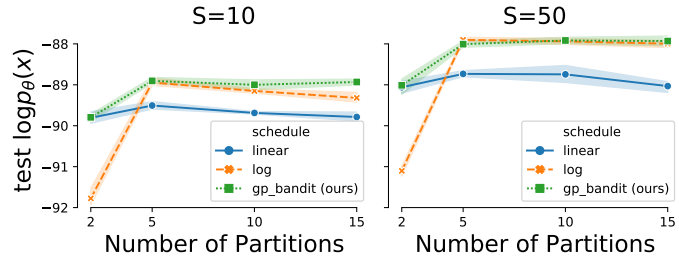


Figure 1: VAE MNIST, 6k epochs, 5 seeds

24 **Figure 2 clarity:** We agree with R2 and R4 that a more thorough description of both Fig. 2 and Fig. 3 are needed.
25 In Fig. 2, we investigate the bandit exploration / exploitation behavior at early, middle, and late stages of training by
26 showing where the bandit positions a single β_1 . Color encodes timestep, so clusters of similar colors indicate the bandit
27 is "exploiting" a particular region, particularly in regions where the blue line, i.e. GP mean, is high. This indicates
28 that our reward model expects the TVO objective will improve with this choice of β_1 . We also show the variance of
29 our GP surrogate model across training phases and see both the mean and variance of predicted reward decreases as
30 optimization converges.

31 The key takeaway from this figure is that we see the bandit exploits early on in training, and that the surrogate reward
32 function correctly learns that the reward for choosing the correct location decreases as optimization proceeds and the
33 curve flattens.

34 **Figure 3 clarity:** R2 correctly observes that it is difficult to know the shape of the integrand. We agree, and this is in
35 fact one of our primary motivations for using a bandits schedule, as bandit optimization is uniquely suited to scenarios
36 where one has little knowledge of the form of the reward function. We show possible example shapes for the integrand
37 in the subpanel of Fig. 3, reflecting bandit choices of β in the middle (orange) and late (green) stages of training. These
38 are based on the intuition that β choices should be concentrated in regions where the integrand is changing quickly,
39 allowing the left Riemann approximation to capture the most area with a fixed budget of d partitions. We also assume
40 that a perfectly flat curve will result in uniform β choices. We will update the caption of Fig. 3 to make this clear.

41 **(R4) Comparison with Bogunovic et. al [5]:** We agree that the positioning of our contribution with respect to [5]
42 requires further clarification, and regret this oversight. Theorem 1 improves the bound on the maximum mutual
43 information gain $\tilde{\gamma}$ from [5] by using Cauchy Schwarz and Jensen's inequality rather than an analysis of the optimality
44 conditions (cf. eq. 61 in [5]). We have updated the main text in 4.3 to make it clear that Theorem 1 follows by using
45 our tighter bound on $\tilde{\gamma}$ in Theorem 4 of [5], and simplified the derivation in the appendix to refer to [5] directly where
46 possible.

47 **(R4) Discussion on spatial covariance:** R4 asks for clarification on covariance functions which can be used alongside
48 our projection operation. Since the projection preserves the input space, any PSD covariance function will maintain this
49 property after projection. We recommend choosing a kernel for which bounds on the maximum information gain are
50 known, such as exponentiated quadratic, Matern, or linear from Srinivas et al 2010 [35].

51 **Typos:** R1, R3, R4 helpfully point out a number of typos and suggestions to improve the writing which we will
52 incorporate into the final draft.

53 **(R4) Ref [43] in the supplement:** Martin J Wainwright. "Basic concentration bounds." In *High-dimensional Statistics:*
54 *A non-asymptotic viewpoint*. Chapter 2, pages 21–57. 2019